Journal of Non-Newtonian Fluid Mechanics, 21 (1986) 79–97
Elsevier Science Publishers B.V., Amsterdam – Printed in The Netherlands

NONLINEAR ANALYSIS OF THE SURFACE TENSION DRIVEN BREAKUP OF VISCOELASTIC FILAMENTS

D.W. BOUSFIELD, R. KEUNINGS, G. MARRUCCI and M.M. DENN

Lawrence Berkeley Laboratory and Department of Chemical Engineering, University of California, Berkeley, CA 94720 (U.S.A.)

(Received October 14, 1985)

Summary

The surface tension driven breakup of viscoelastic filaments into droplets is qualitatively different from that of Newtonian liquid filaments. Disturbances on filaments of dilute polymer solutions often grow to a configuration consisting of nascent droplets connected by a thin ligament; the breakup time for this configuration is much longer than that predicted by extensions of Rayleigh's linear stability theory. We present here a nonlinear analysis of surface tension driven breakup of viscoelastic filaments using two complementary approaches that give equivalent results: a transient finite element solution and a one-dimensional thin filament approximation. We show that significant nonlinear effects lead to the experimentally-observed nascent droplet–ligament configuration, and we predict the entire evolution of the filament profile. Agreement with available experimental data for profile evolution and breakup of jets of Newtonian fluids and dilute polymer solutions is excellent.

Introduction

The surface tension-driven breakup of a liquid filament into droplets is an important step in a variety of processes. Applications in a wide range of industries have recently been enumerated by Schümmer and Tebel [1]. The mechanisms governing the breakup of filaments of Newtonian fluids seem generally to be understood; the subject has been broadly reviewed by Bogy [2] and McCarthy and Molloy [3]. This is not the case for the breakup of filaments of polymeric liquids. It is observed experimentally that jets of polymer solutions generally take longer to break up into droplets than jets of purely viscous liquids of comparable shear viscosity; sometimes breakup

0377-0257/86/$03.50

does not occur at all [4]. This phenomenon is usually interpreted in terms of the known large resistance of polymer solutions to elongational stretching deformations, but the concept has not been quantified through an analysis of the fluid mechanics.

The breakup of liquid filaments was first analyzed by Rayleigh [5] using linear stability theory. Rayleigh assumed an equivalence between spatial and temporal growth of disturbances, and thus calculated the growth of infinitesimal periodic disturbances on a stationary liquid cylinder. This approach precludes any consideration of velocity profile rearrangement on the jet in the neighborhood of the nozzle, and it assumes that the disturbance wavelength remains constant as the disturbance evolves. Most subsequent investigators have followed Rayleigh's basic approach, and have thus been limited to the early stages of disturbance growth. The notable exception has been the recent work of Bogy and others [6] using a one-dimensional Cosserat director theory or the equivalent to study the nonlinear mechanics, enabling prediction of the development of satellite droplets in the absence of viscosity. The Cosserat theory used by Bogy is developed *ab initio* as a one-dimensional theory [7] and contains other one-dimensional approximations obtained from the full Navier–Stokes equations as special cases.

The linear stability analysis has been carried out for a general linear viscoelastic liquid [4,8]. This result is in fact general for any Simple Fluid, since the disturbance is about the rest state and the strains are infinitesimal. The conclusion is that in all cases a disturbance will grow more rapidly on a viscoelastic filament than on a Newtonian filament with the same shear viscosity. This result is expected, since the initial resistance to deformation of a viscoelastic liquid is always less than for the corresponding Newtonian liquid. The linear theory has often been interpreted as being inconsistent with the experimental observations of a longer time to breakup, but this is simply the result of an inappropriate application of a linear theory to an inherently nonlinear phenomenon. Goren and Gottlieb [9] have argued that unrelaxed tensile stresses generated in the nozzle may explain the retarded breakup, and have repeated the linear analysis including such terms. Large initial tensile stresses will delay the initial growth, but are unlikely to be relevant to the ultimate breakup mechanism.

We present here the results of a dynamical analysis of the growth of surface tension-driven disturbances on thin filaments of Newtonian and viscoelastic liquids. The results incorporate the linear theory during the early stages of disturbance growth, but they include the system nonlinearities and are also valid at long times approaching filament breakup. Two complementary approaches have been used, giving the same result. One is a new Galerkin/finite element numerical algorithm for solving transient free-surface flows of viscoelastic liquids; the algorithm is described in detail

elsewhere [10]. The other is a one-dimensional theory for viscoelastic filaments obtained by averaging the momentum equation over the filament cross section at each axial position, in much the same way as has traditionally been done in the analysis of fiber spinning [11], but retaining the finite curvature in the one-dimensional equations. Preliminary results of these analyses were summarized in the Proceedings of the IX International Congress of Rheology [12,13]. The major conclusion is that disturbances on viscoelastic jets do grow more rapidly at short times than on Newtonian jets, as predicted by linear stability theory, but there is a retardation of the disturbance growth and stabilization of the viscoelastic jets at long times as a consequence of the buildup of large extensional stresses. Nonlinearities associated with inertial stresses lead to the development of the satellite droplets often observed on Newtonian jets (e.g. [14–18]), and satellite droplet formation is retarded by the effect of elasticity. A residual tensile stress from the nozzle will delay the initial disturbance growth, but the stabilization due to the buildup of extensional stresses controls the final breakup mechanism and, ultimately, the breakup time.

Formulation

We assume that an infinitely-long uniform liquid cylinder of initial radius R_0 is perturbed slightly with a periodic axi-symmetric disturbance of wavelength $2L$. The wavelength is then assumed to remain constant as the surface tension-driven disturbance grows in time. This assumption is consistent with photographic evidence of the breakup of filaments forced with a constant frequency, as shown in Fig. 1 [14,19]. We further assume for convenience that the initial disturbance is symmetric about the midpoint, so only one-half wavelength need be considered. This assumption only approximates the observed spatial growth of the disturbance; it reduces the scope of the problem considerably and is not expected to be a serious restriction.

The geometry is shown schematically in Fig. 2. The flow field is defined by the axi-symmetric Cauchy momentum equation (neglecting gravity) and the appropriate stress constitutive equations. The following kinematical and stress conditions hold at the free surface:

$$\frac{\partial R}{\partial t} + U\frac{\partial R}{\partial z} = V, \tag{1}$$

$$(-p\boldsymbol{I} + \boldsymbol{T}) \cdot \boldsymbol{n} = \sigma \left\{ \frac{R\dfrac{\partial^2 R}{\partial z^2} - \left(\dfrac{\partial R}{\partial z}\right)^2 - 1}{R\left[1 + \left(\dfrac{\partial R}{\partial z}\right)^2\right]^{3/2}} \right\} \boldsymbol{n}. \tag{2}$$

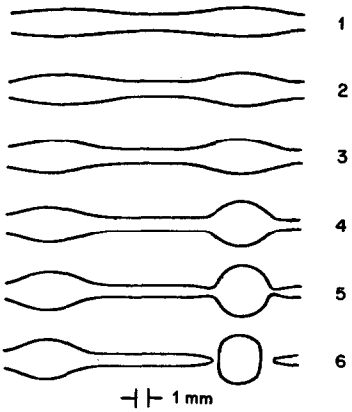

Fig. 1. Stages in the breakup of a Newtonian jet; after photographic data of Goedde and Yuen [14]. Successive frames are separated by 1.25×10^{-3} s.

U and V are the axial and radial components, respectively, of the velocity vector $\boldsymbol{V}$, and $\boldsymbol{T}$ is the extra-stress; σ is the surface tension. Symmetry requires the following conditions at $z = 0$ and L:

$$U = \frac{\partial V}{\partial z} = \frac{\partial R}{\partial z} = 0. \tag{3}$$

The extra-stress for the viscoelastic liquid is described by the Oldroyd-B or Maxwell models. The former includes the latter as a special case and is given by

$$\boldsymbol{T} + \lambda_p \frac{\delta \boldsymbol{T}}{\delta t} = 2\eta \left(\boldsymbol{D} + \lambda_r \frac{\delta \boldsymbol{D}}{\delta t} \right), \tag{4a}$$

$$\boldsymbol{D} = \tfrac{1}{2}\left[\nabla \boldsymbol{V} + (\nabla \boldsymbol{V})^{\dagger} \right], \tag{4b}$$

$$\frac{\delta(\ )}{\delta t} = \frac{\partial(\ )}{\partial t} + \boldsymbol{V} \cdot \nabla(\ ) - (\nabla \boldsymbol{V})^{\dagger} \cdot (\ ) - (\ ) \cdot \nabla \boldsymbol{V}. \tag{4c}$$

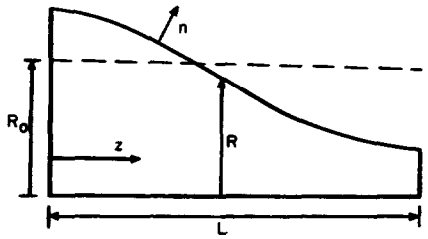

Fig. 2. Schematic of a deforming liquid filament.

λ_p is the polymer relaxation time, η is the viscosity, and λ_r is the retardation time. The Maxwell fluid corresponds to $\lambda_r = 0$, while the Newtonian fluid limit is recovered for $\lambda_p = \lambda_r$. Equation (4) is derivable from molecular theory as a first approximation to the stress in a polymer solution, with $\lambda_r = \lambda_p \eta_s / \eta$, where η_s is the viscosity of the solvent.

All results are expressed in terms of a set of dimensionless variables that are natural to the problem, as follows:

$$r = R/R_0, \quad \zeta = z/L, \quad \theta = \sigma t/\eta R_0.$$

Four dimensionless parameters characterize the system,

$$\alpha = R_0/L, \quad \beta = \left(\frac{\rho\sigma R_0}{\eta^2}\right)\left(\frac{L}{R_0}\right)^2, \quad \phi = \lambda_p \sigma/\eta R_0, \quad \Lambda = \lambda_r/\lambda_p.$$

α accounts for finite curvature; β is a measure of the inertial stresses relative to surface tension; $\eta^2/\rho\sigma R_0$ is the square of the Ohnesorge number. $\phi(1-\Lambda)$ is a measure of viscoelasticity, and might be considered a Deborah number for the disturbance growth; in the Maxwell limit ($\Lambda = 0$) ϕ is the ratio of surface tension stresses to the elastic shear modulus.

Solution

Calculations using either the finite element or thin filament approaches were usually begun with an initial dimensionless radius profile

$$r = 1 + \epsilon \cos \pi\zeta, \tag{5}$$

with ϵ typically equal to 0.05. This is sufficient to define the complete initial state in the absence of inertia and elasticity ($\beta = \phi = 0$). The profile will, of course, lose the sinusoidal character when nonlinear effects become important. For β or ϕ different from zero the initial velocity and extra-stress must also be specified. The particular choice determines the nature of the

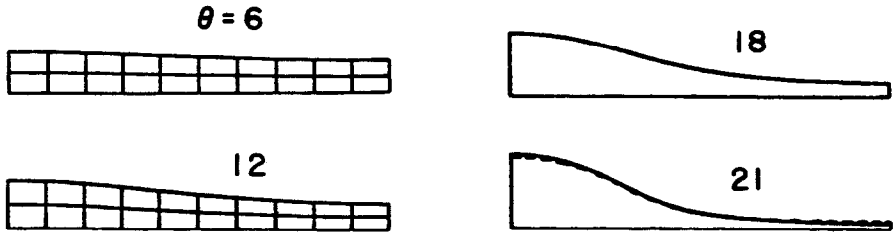

Fig. 3. Disturbance growth on a Newtonian filament, $\epsilon = 0.05$, $\alpha = 0.10$, $\beta = 0$, using the finite element code. The dashed line at $\theta = 21$ is the solution using the thin filament approximation.

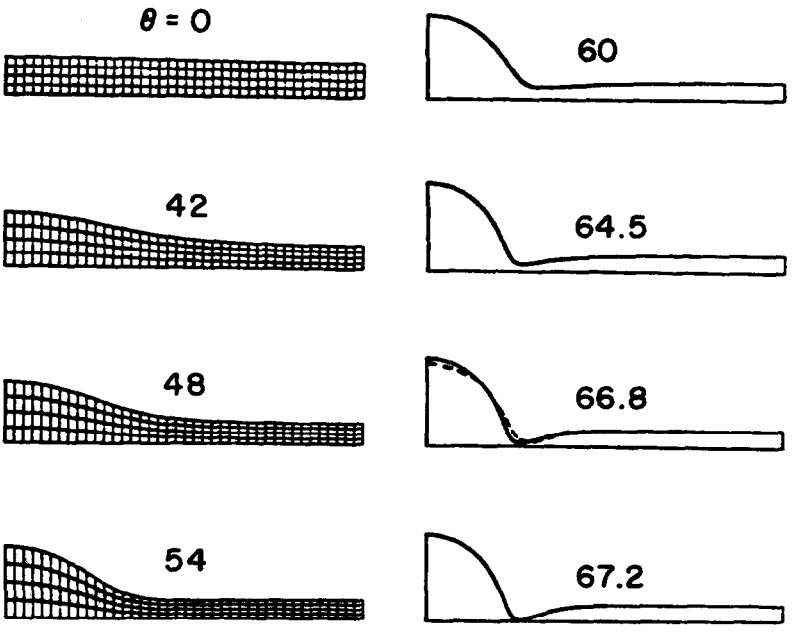

Fig. 4. Disturbance growth on a Newtonian filament, $\epsilon = 0.05$, $\alpha = 0.10$, $\beta = 1080$, using the finite element code. The dashed line at $\theta = 66.8$ is the solution using the thin filament approximation.

initial portion of the transient, before the fastest growing linear mode begins to dominate or nonlinear effects take over. The initial velocity and stress distribution corresponding to the linearized solution of the momentum equation with the radial profile given by eqn. (5) must be used if direct comparison is to be made with linear stability theory; this velocity and stress distribution is given in an appendix to Keunings [10].

The transient finite element algorithm is described in detail in Keunings [10]. Figures 3 and 4 show the computed flow domain and the finite element mesh for a Newtonian jet with $\epsilon = 0.05$, $\alpha = 0.10$, and $\beta = 0$ and 1080, respectively. The latter value is typical of the experiments on aqueous glycerol solutions by Goedde and Yuen [14].

The thin filament equations are presented in Appendix A. The dashed lines defining flow domains in Figs. 3 and 4 at $\theta = 21$ and $\theta = 66.8$, respectively, are the computed results from the thin filament equations. Clearly, agreement between the two methods is excellent. This comparison justifies the use of the thin filament equations for parametric studies, since their numerical solution is much less costly than solutions using the finite element code.

Newtonian fluids

The effect of inertia relative to viscosity is dramatically illustrated by comparison of Figs. 3 and 4. Disturbance growth on the highly viscous filament is much more rapid (in units of dimensionless time which, it must be remembered, scales with η^{-1}). The thinnest point on the viscous jet is always at the midpoint between the nodes (which we denote as the *neck*), and thus uniform droplets of volume $2\pi R_0^2 L$ are expected at breakup. The thinnest point moves away from the neck when inertia is important, and breakup will occur as primary drops with connecting ligaments; the ligaments will form satellite drops if no post-merging with a primary drop occurs. This highly nonlinear phenomenon is indeed what is observed experimentally, and Fig. 4 agrees remarkably well with photographs of glycerol/water jets taken by Goedde and Yuen [14].

It is convenient to plot the logarithm of the disturbance amplitude, $|r-1|$, versus time in order to make comparisons with the linear theory. This quantity has a value $\epsilon|\cos \pi\zeta|$ at $\theta = 0$, and will equal unity if $r = 0$. The intercept when $\theta = 0$ is equal to ϵ both at the point of maximum swell ($\zeta = 0$) and at the neck ($\zeta = 1$), with a value less than ϵ at all points in between. According to the linear stability theory a semi-logarithmic plot of disturbance amplitude will be a straight line with slope γ, where γ is the dimensionless growth rate for the given wavelength. γ is given by the solution of an implicit algebraic equation (see Appendix B) in which α and β appear as parameters.

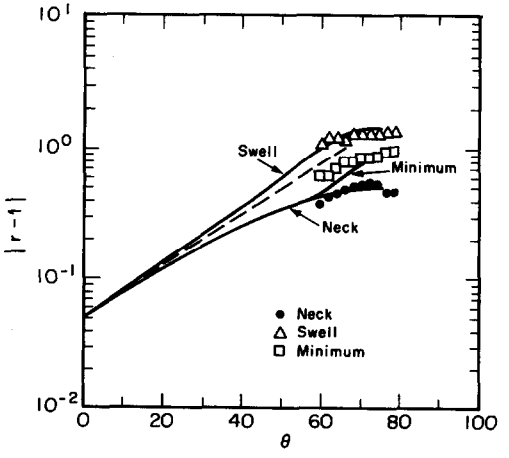

Fig. 5. Computed disturbance amplitude for a glycerol/water jet, $\alpha = 0.094$, $\beta = 1400$. The intercept at $\theta = 0$ is determined by fitting data of Goedde and Yuen [14]. The dashed line is the amplitude from linear stability theory.

Figure 5 shows the computed disturbance amplitude for $\alpha = 0.094$, $\beta = 1400$ at the swell, the neck, and at the thinnest point between, which moves from the neck at $\theta = 0$ to $\zeta = 0.4$ at breakup. These parameters correspond to a particular experiment of Goedde and Yuen [14]. The dashed line is the disturbance computed from the linear stability analysis. The linear theory agrees well with the nonlinear analysis at short times, as it must, but substantial deviations begin to occur at $\theta = 50$. Mass is conserved in the linear theory only to order ϵ, and large errors in mass conservation also result from the linear theory calculations beyond this point. Breakup is always predicted to occur at the neck in the linear theory; the breakup time computed by extrapolating the linear curve to $|r - 1| = 1$ does not differ significantly from that computed using the nonlinear theory, despite the gross error in shape. This agreement in the predicted time to breakup occurs because of a cancellation of second order terms.

The data in Fig. 5 are taken from photographs published by Goedde and Yuen [14] for the breakup of glycerol/water jet. The close agreement at the three points (swell, neck, and thinnest point) shows that the nonlinear jet profile has been computed correctly at breakup. It is notable, however, that none of the data lie in the linear regime. There is therefore no way of computing the initial perturbation amplitude, and the data set can be shifted horizontally in the absence of information about the time-of-flight from the nozzle (which is not given).

The data in Fig. 6 for a water jet are taken from analyzed photographs in the thesis of Chin [20], who studied the breakup of horizontal jets. The disturbance was introduced by vibration of the nozzle. The location of the

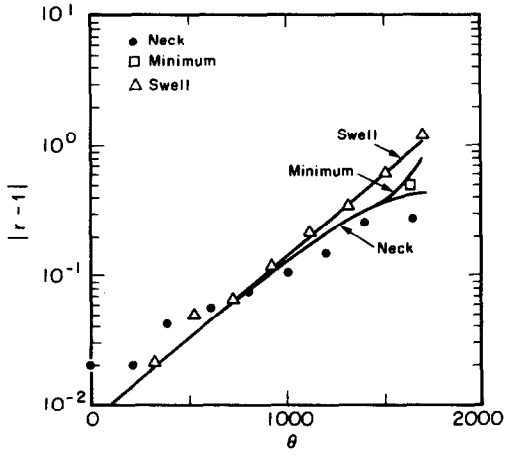

Fig. 6. Computed disturbance amplitude for a water jet, $\alpha = 0.1355$, $\beta = 4.11 \times 10^5$. The intercept at $\theta = 0$ is determined by fitting data of Chin [20] in the linear region.

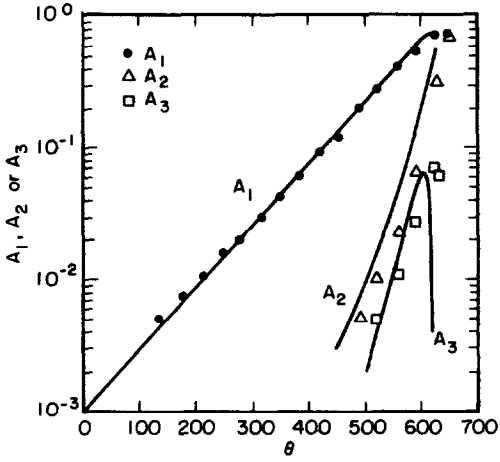

Fig. 7. Computed amplitudes of first three harmonics of disturbance on a water/ink jet, $\alpha = 0.19$, $\beta = 2.5 \times 10^4$. The intercept of A_1 at $\theta = 0$ is determined by fitting data of Taub [15] in the linear region.

jet centerline ($\zeta = 0$) was computed by accounting for "droop" because of gravity. The experimental parameters were $\alpha = 0.1355$, $\beta = 4.11 \times 10^5$. Only the intercept at $\theta = 0$, corresponding to the initial perturbation of $\epsilon = 0.0073$, was fit in these calculations.

Taub [15] reported the evolution of the shape of a water/ink jet in terms of the temporal growth of the Fourier coefficients in an expansion in the

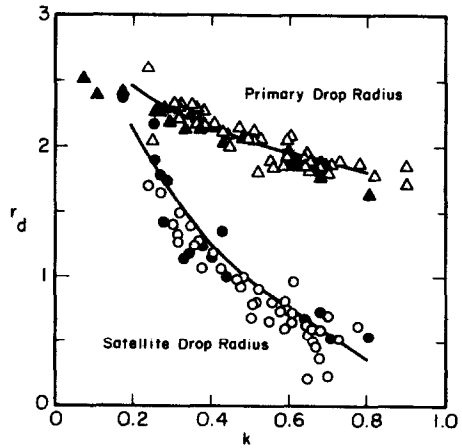

Fig. 8. Computed radii of primary and satellite drops for water jets as a function of disturbance wavenumber. The filled symbols are data of Rutland and Jameson [17] and the open symbols are data of Lafrance [18].

form

$$r = 1 + A_1(\theta) \cos \pi\zeta + A_2(\theta) \cos 2\pi\zeta + A_3(\theta) \cos 3\pi\zeta + \ldots. \quad (6)$$

Figure 7 shows some of Taub's data and the computed result for $\alpha = 0.19$, $\beta = 2.5 \times 10^4$, which corresponds to a water jet with $R_0 = 0.0159$ mm, $L = 0.084$ mm, $\eta = 1$ cp, $\rho = 1$ g/cm^3, and $\sigma = 55.7$ dyne/cm. (The surface tension was determined by Taub by fitting several sets of data to Yuen's [16] nonlinear analysis.) The initial perturbation $\epsilon = 10^{-3}$ is fit by extrapolating the linear curve (A_1) to $\theta = 0$; there are no other adjustable parameters. The agreement with the measured higher harmonics is excellent. Improvements over Yuen's analysis are apparent near breakup, both in predicting breakup time and in the details of the Fourier coefficient behavior.

Figure 8 shows the radius r_d (made dimensionless with R_0) of the primary and satellite drops produced for different disturbance wavenumbers k, where $k = \pi\alpha$. The data are from Rutland and Jameson [17] and Lafrance [18]. The lines are the drop sizes predicted from the nonlinear analysis using the fluid properties of water and $\epsilon = 0.01$. Final drop sizes are well predicted by the analysis.

Viscoelastic liquids

A comparison between disturbance growth on Newtonian jet and on a jet of an Oldroyd-B fluid is shown in Fig. 9 for $\alpha = 0.1$, $\beta = 0$; the viscoelastic parameters are $\phi = 30$, $\Lambda = 0.25$. To the extent that the Oldroyd-B theory models real systems, this would correspond to a 1 mm radius jet of an aqueous polymer solution with $\lambda_p = 0.17$ s. (A ratio $\eta_s/\eta = 0.25$ is outside the range of validity of the dilute solution theory, however.) Consistency with the given value of ϕ requires $\beta = 45$, which is negligibly small, and the calculations were therefore done for $\beta = 0$ in order to examine the effect of fluid elasticity without inertia. These calculations were carried out using the finite element analysis; nearly identical results are obtained using the thin filament theory up to $\theta = 8$, after which numerical instability is encountered for the viscoelastic liquid with the spatial resolution employed. Initial conditions for the velocity and stress were taken to be those for inertialess flow of a Newtonian liquid.

The disturbance initially grows much more rapidly on the viscoelastic filament, completely in accordance with our expectations and with the linear theory. For value of θ greater than nine the shape of the viscoelastic jet is nearly stabilized into the nascent droplet–connecting ligament configuration seen experimentally; the disturbance continues to grow on the Newtonian filament, however. The Newtonian filament breaks up for θ slightly greater than 21, while there is virtually no further deformation of the viscoelastic filament as seen on this time scale.

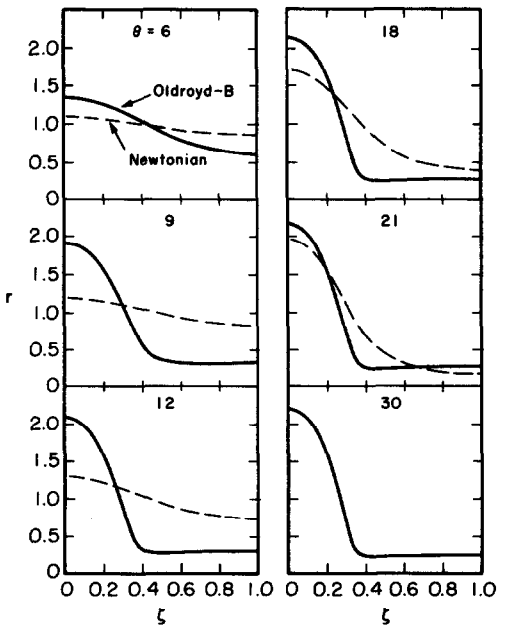

Fig. 9. Computed disturbance growth for $\alpha = 0.1$, $\beta = 0$, on jets of a Newtonian fluid (dashes) and an Oldroyd-B fluid (solid) with $\phi = 30$, $\Lambda = 0.25$.

Figure 10 shows the disturbance amplitude for the viscoelastic liquid at the swell and at the neck (which remains the thinnest point for $\beta = 0$), computed with the finite element code using initial conditions consistent

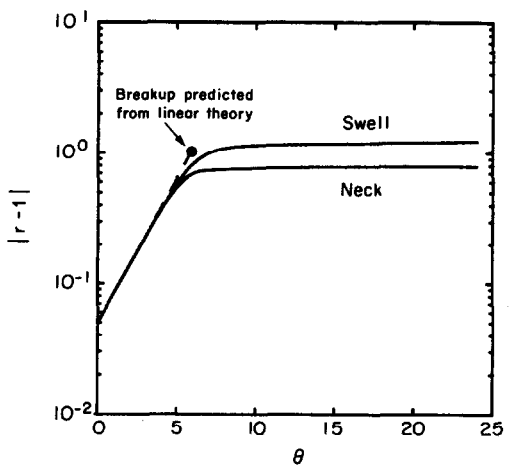

Fig. 10. Computed disturbance amplitude for a jet of an Oldroyd-B fluid, $\alpha = 0.1$, $\beta = 0$, $\phi = 30$, $\Lambda = 0.25$. The dashed line is the amplitude from linear stability theory.

with the linear stability analysis (Appendix B); the dashed line shows the disturbance growth given by the linear stability analysis. Agreement with the linear theory is excellent up to about $\theta = 4$. There is a sharp transition thereafter, however, and whereas extrapolation of the linear theory would predict breakup at $\theta \approx 6$, breakup does not occur at all over the time scale for which the calculations were carried out.

The formation of satellite droplets is suppressed when inertial effects are present in viscoelastic filaments. The initial disturbance growth is again identical to that predicted by the linear stability analysis, but the subsequent shape develops as though a satellite drop will form, as in Fig. 4. Viscoelastic effects hinder the separation of the ligament from the primary drop, however.

The rheological model used here has a constant shear viscosity, while the polymer solutions used in breakup studies have usually been shear thinning. The qualitative features of the nonlinear mechanics will remain unchanged, however. There is no contradiction between the linear stability analysis and the experiments, but any attempt to apply the linear theory to a breakup calculation is clearly inappropriate.

Asymptotic behavior

The viscoelastic filament is often observed experimentally to approach an apparently stable configuration that can be approximated by two large droplets connected by a long cylinder of uniform radius. Figure 11 is taken from Goldin et al. [4], for example. The pressure in the droplets can be taken to be approximately atmospheric, in which case the thin filament equations simplify to the equation describing uniform uniaxial extension of a viscoelastic cylinder as a result of radial compressive stresses resulting from surface tension. The radius of the cylinder of a Maxwell fluid decreases uniformly according to the equation

$$\phi \frac{\ddot{r}}{\dot{r}} + 9\phi^2 \left(\frac{\dot{r}}{r}\right)^2 - \phi \frac{\dot{r}}{r} - 6\dot{r} - 1 = 0. \tag{7}$$

Equation (7) is equivalent to a special case of eqn. (66) of Schümmer and Tebel [1]. The Newtonian fluid is recovered in the limit $\phi \to 0$, with a solution

$$\phi \to 0: \quad r \to \text{constant} - \theta/6. \tag{8}$$

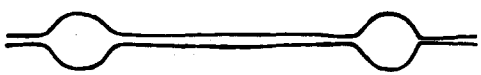

Fig. 11. Shape of a jet of a polymer solution, after Goldin et al. [4].

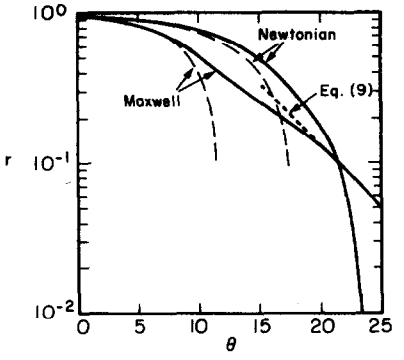

Fig. 12. Computed dimensionless radius at the neck, $\beta = 0$, for jets of a Newtonian fluid and a Maxwell fluid ($\Lambda = 0$) with $\phi = 2$. The Maxwell fluid approaches the asymptotic behavior defined by eqn. (9).

An analytical solution is not available for the Maxwell fluid, but for $\theta \gg \phi$ the long time asymptote is obtained as

$$\theta \gg \phi: \quad \ln r \to \text{const} - \theta/3\phi. \tag{9}$$

It is clear from the asymptotic behavior for the two fluid models that a Newtonian filament in this configuration would rupture in a finite time of order $\theta = 6$ ($t = 6\eta R_0/\sigma$), while a viscoelastic filament would thin much more slowly; the exponential approaches zero for $\theta \sim 9\phi$, corresponding to $t \sim 9\lambda_p$. The latter time is longer than the Newtonian breakup time scale provided $\phi \gg 1$, which is therefore the condition for viscoelastic dominance of the breakup process.

This asymptotic behavior can be seen in Fig. 12, where the dimensionless radius at the neck is plotted versus time for $\beta = 0$ for a Newtonian filament and for a Maxwell liquid with $\phi = 2$. The broken lines are the linear stability analysis. The figure graphically illustrates the more rapid disturbance growth

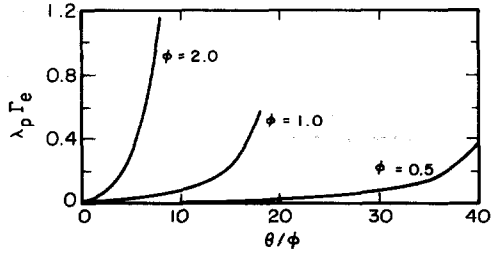

Fig. 13. Computed dimensionless stretch rate at $\zeta = 0.4$ as a function of dimensionless time for a Maxwell fluid. Note that $\theta/\phi = t/\lambda_p$.

for the viscoelastic liquid, followed by the transition to the asymptotic exponential decay defined by eqn. (9). In contrast, the Newtonian filament breaks up in a finite time.

The stabilization of filaments of polymer solutions is usually attributed to a resistance to extensional deformations with stretch rates of the order of $\frac{1}{2}\lambda_p$ and greater (e.g. [19]); this is the value at which extensional stresses grow without bound for a Maxwell liquid for times that are long relative to λ_p [21]. The computed stretch rate Γ_e at $\zeta = 0.4$ for disturbance growth on a filament of a Maxwell liquid, $\phi = 2$ and $\beta = 0$, is shown in Fig. 13. Clearly the long-time stabilization corresponds to the rapid growth of $\lambda_p\Gamma_e$. It is this nonlinear behavior resulting from the buildup of extensional stresses that inhibits the breakup of viscoelastic jets.

Non-zero tensile stresses

Goren and Gottlieb [9] have argued that unrelaxed tensile stresses generated during extrusion will retard the disturbance growth, and they have repeated the linear stability analysis for an Oldroyd 8-constant fluid with non-zero initial values of the tensile stresses. There is an approximation in their analysis, where they assume that stress relaxation is slow relative to disturbance growth, and hence $\gamma\lambda_p \gg 1$.

A non-zero initial stress can be incorporated in the nonlinear analysis without approximation. One additional parameter, denoted T_e, is intro-

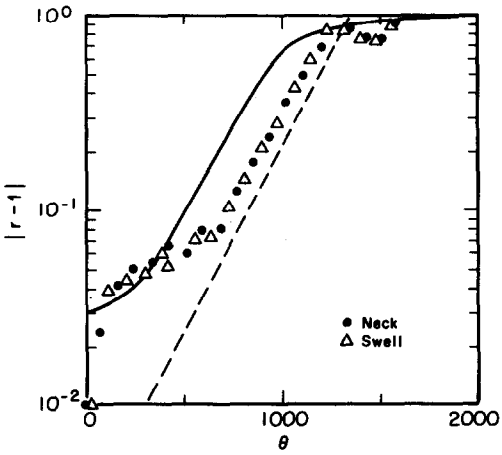

Fig. 14. Computed disturbance amplitude for a jet of 50 ppm Polyox WSRN-12K in water, $\alpha = 0.2$, $\beta = 1.47 \times 10^5$, $\Lambda = 0.96$, $\phi = 116.7$, $T_e = 0.47$. The dashed line is the slope of the amplitude from linear stability theory following relaxation of the initial stress. The intercept $\epsilon = 0.03$ at $\theta = 0$ is determined by fitting data of Chin [20].

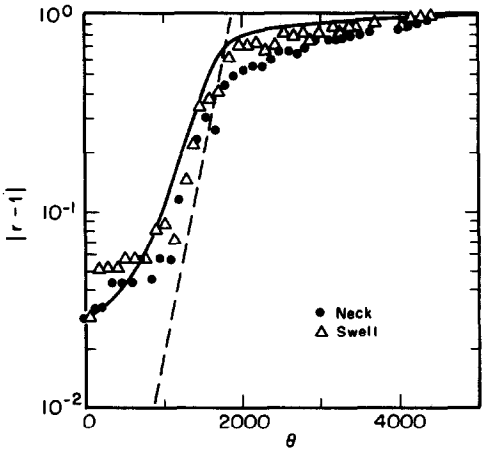

Fig. 15. Computed disturbance amplitude for a jet of 25 ppm Polyox WSRN-60K in water, $\alpha = 0.2$, $\beta = 1.47 \times 10^5$, $\Lambda = 0.96$, $\phi = 475$, $T_e = 1.76$. The dashed line is the slope of the amplitude from linear stability theory following relaxation of the initial stress. The intercept $\epsilon = 0.03$ at $\theta = 0$ is determined by fitting data of Chin [30].

duced; this is the tensile stress at $\theta = 0$ normalized with respect to σ/R_0. Goren and Gottlieb's linear theory, when valid, gives results at short times that are identical to those obtained from the thin filament theory. The linear theory cannot describe the nonlinear effects at long time, however, and predicts breakup times that are too short.

Figures 14 and 15 show data from the thesis of Chin [20] for aqueous solutions of 50 wppm Polyox WSRN-12K and 25 wppm Polyox WSRN-60K, respectively. The measured surface tension was 64.9 dyne/cm and the measured solution viscosity was 1.04 cp for both solutions. λ_p was computed from the molecular theory of Williams [22] to be 1.9×10^{-4} s and 7.8×10^{-4} s, respectively. The vibrating nozzle of radius $R_0 = 0.102$ mm produced a wavelength $2L$ of 1 mm. These properties and dimensions correspond to $\alpha = 0.2$, $\beta = 1.47 \times 10^5$, and $\Lambda = 0.96$, with $\phi = 116.7$ for Fig. 14 and $\phi = 475$ for Fig. 15. The scatter near $\theta = 0$ may reflect the difficulty of measuring small perturbation quantities, but it might be related to the imposition of a finite oscillatory initial velocity [23].

The initial dimensionless tensile stress T_e was computed using the cup (flow rate) average for fully-developed tube flow:

$$T_e = \frac{32(1-\Lambda)}{3\phi}\left(\frac{\lambda_p \bar{V}}{R_o}\right)^2, \tag{10}$$

where $\bar{V}$ is the average velocity. This calculation neglects the effect of flow rearrangement near the tube exit [24], but is should give a reasonable

estimate of the correct order. The computation using the nonlinear theory is shown as the solid line in Figs. 14 and 15. The only adjustable parameter is the initial disturbance amplitude, which was taken to be $\epsilon = 0.03$ to fit the data as θ approaches zero. The same value was used for both experiments, since the same voltage was applied to vibrate the nozzle. The calculation was carried out until the asymptotic behavior described by eqn. (9) was reached, after which the curve was extended using the asymptotic theory.

The analysis fits the experimental data extremely well. Similar results are obtained for the remainder of Chin's data; see Bousfield [25]. Even better agreement can be obtained by varying T_e by up to 40 percent, which is well within the uncertainty of the estimate, but this does not seem warranted by the precision of the data. The dashed line shows the slope computed from the linear growth rate without considering the initial stress. The Goren and Gottlieb theory is not applicable for these parameters and is not shown.

Stress relaxation and linear growth are seen to occur on comparable time scales, and there is a region of approach to the constant growth rate computed from linear theory. The viscoelastic nonlinearity dominates the breakup, however, and extrapolation of the linear theory would greatly underestimate the breakup time.

Conclusion

The breakup of a liquid filament into droplets is an inherently nonlinear phenomenon, which can be described both by numerical solution of the full momentum and constitutive equations and by one-dimensional "thin filament" analysis. The theory is completely predictive, requiring only the initial perturbation. The initial surface tension-driven deformation grows much more rapidly on polymeric filaments than on filaments of Newtonian liquids, but the extensional stresses stabilize the viscoelastic filaments and retard breakup. Inertia causes the formation of satellite droplets in low viscosity liquid jets; viscoelasticity acts to retard satellite droplet formation and to maintain the thinnest point on the filament at the midpoint between droplets. A residual tensile stress from the nozzle flow will retard the initial disturbance growth, but the nonlinear extensional stresses control the final breakup mechanism.

Appendix A

Thin filament equations

The thin filament equations are derived by averaging the axi-symmetric momentum equations over the filament cross-section at each axial position,

with the assumption that the axial velocity U is a function only of the axial coordinate, z, and that radial inertial terms can be neglected. Details are contained in Bousfield [25]. The equations for a Newtonian fluid are obtained as follows:

$$\dot{r} = (E + F)/6r, \tag{A1}$$

$$F = -\int_0^1 E/r^2 \, d\zeta \Big/ \int_0^1 1/r^2 \, d\zeta, \tag{A2}$$

$$E = -\beta \int_0^\zeta r^2 \dot{u} \, d\zeta + r\left(1 + \alpha^2 r_\zeta^2\right)^{-1/2} + \alpha^2 r^2 r_{\zeta\zeta}\left(1 + \alpha^2 r_\zeta^2\right)^{-3/2}, \tag{A3}$$

where

$$\dot{r} = r_\theta + u r_\zeta, \tag{A4a}$$

$$\dot{u} = u_\theta + u u_\zeta, \tag{A4b}$$

$$u = -2\int_0^\zeta r^{-1}\dot{r} \, d\zeta. \tag{A4c}$$

Subscripts denote partial differentiation. These equations are equivalent to a spatial integration of the Cosserat director theory used by Bogy [6], eqn. 8), except that the radial inertial terms and one viscous term, $\eta(R^2 v_{zz})_z$, are not included.

For an Oldroyd-B fluid, the thin filament equations are

$$\dot{r} = \frac{(G + H + I + J)r}{2(K - M)}, \tag{A5}$$

$$G = -\frac{\int_0^1 (H + I + J)/(K - M) \, d\zeta}{\int_0^1 1/(K - M) \, d\zeta}, \tag{A6}$$

$$H = -\beta\phi \int_0^\zeta r^2\left(u_{\theta\theta} + 2u u_{\theta\zeta} + u^2 u_{\zeta\zeta}\right) d\zeta - \beta \int_0^\zeta r^2 \dot{u} d\zeta, \tag{A7}$$

$$I = -\frac{\alpha^2 \phi r r_\zeta r_{\zeta\theta}}{\left(1 + \alpha^2 r_\zeta^2\right)^{3/2}} - \frac{\alpha^2 \phi r^2 r_{\zeta\zeta\theta}}{\left(1 + \alpha^2 r_\zeta^2\right)^{3/2}} - \frac{3\alpha^4 \phi r^2 r_{\zeta\zeta} r_\zeta r_{\zeta\theta}}{\left(1 + \alpha^2 r_\zeta^2\right)^{5/2}}, \tag{A8}$$

$$J = \frac{r}{\left(1 + \alpha^2 r_\zeta^2\right)^{1/2}} + \frac{\alpha^2 r^2 r_{\zeta\zeta}}{\left(1 + \alpha^2 r_\zeta^2\right)^{3/2}} - 6\phi\Lambda(r\ddot{r} - \dot{r}^2), \tag{A9}$$

$$K = \phi r^2(\tau_{11} + 2\tau_{22}) + 3r^2 + 6\phi\Lambda r\dot{r}, \tag{A10}$$

$$M = \frac{\phi r}{2\left(1 + \alpha^2 r_\zeta^2\right)^{1/2}} - \frac{\alpha^2 \phi r^2 r_{\zeta\zeta}}{\left(1 + \alpha^2 r_\zeta^2\right)^{3/2}}, \tag{A11}$$

where

$$\ddot{r} = r_{\zeta\zeta} - 2ur_{\zeta\theta} - u_\theta r_\zeta + uu_\zeta r_\zeta + u^2 r_{\zeta\zeta} \tag{A12}$$

and τ_{11} and τ_{22} are extra-stress components in the axial and radial directions, respectively.

Appendix B

Linear stability theory

Disturbances with an initial value given by eqn. (5) grow in the limit $\epsilon \to 0$ as

$$r = 1 + \epsilon \cos \pi\zeta \exp(\gamma\theta). \tag{A13}$$

The growth rate γ is given by the solution of the algebraic equation [4]

$$\gamma + \frac{2\pi^2\bar{\eta}I_1(\pi\alpha)}{\beta}\left[1 - \frac{2\pi(\pi^2 + \lambda\beta/\bar{\eta})^{1/2} I_1(\pi\alpha)}{(2\pi^2 + \gamma\beta/\bar{\eta}) I_1\left((\pi^2 + \gamma\beta/\bar{\eta})^{1/2}\alpha\right)}\right]$$

$$= \frac{\pi(1 - \pi^2\alpha^2) I_1(\pi\alpha)}{\alpha\bar{\eta} I_0(\pi\alpha)(2\pi^2 + \alpha\beta/\bar{\eta})}. \tag{A14}$$

I_n denotes the modified Bessel function of order n. $\bar{\eta}$ is a function of γ; if the linearized shear stress equation is

$$\sum_{n=0} a_n \frac{\partial^n \tau}{\partial t^n} = \eta \sum_{n=0} b_n \frac{\partial^n \Gamma_s}{\partial t^n}, \tag{A15}$$

with Γ_s the shear rate and $a_0 = b_0 = 1$, then

$$\bar{\eta} = \sum_{n=0} b_n \gamma^n \Big/ \sum_{n=0} a_n \gamma^n. \tag{A16}$$

($\eta\bar{\eta}$ is the complex viscosity.)

For the Oldroyd-B fluid,

$$\bar{\eta} = \frac{1 + \lambda_r\gamma}{1 + \lambda_p\gamma}. \tag{A17}$$

The second term on the left of eqn. (A14) vanishes identically in the limit of $\beta \to 0$, and we have

$$\beta \to 0: \quad \gamma = \frac{(1 - \pi^2\alpha^2) I_1(\pi_a)}{2\pi\alpha\bar{\eta} I_0(\pi\alpha)}. \tag{A18}$$

Growth only occurs in this limit for $\alpha < \pi$. For $\alpha \to 0$ we obtain the result

$$\alpha \to 0,\ \beta \to 0: \quad \gamma = \frac{(1 + \gamma\phi)}{6(1 + \gamma\Lambda\phi)}. \tag{A19}$$

We thus recover $\gamma = 1/6$ for the Newtonian fluid, $\gamma \to 1/6\Lambda$ for large ϕ, and

$$\alpha \to 0,\ \beta \to 0,\ \Lambda = 0: \quad \gamma = \frac{1}{6 - \phi} \tag{A20}$$

for the Maxwell fluid.

Acknowledgment

This work was supported by the U.S. Army, ARRADCOM, under Agreement No. 3311-1412 through the U.S. Department of Energy under Contract No. DE-AC03-76SF00098. Roland Keunings was a fellow of the Miller Institute for Basic Research in Science.

References

1 P. Schümmer and K.H. Tebel, Germ. Chem. Eng., 5 (1982) 209.
2 D.B. Bogy, Ann. Rev. Fluid. Mech., 11 (1979) 207.
3 M.J. McCarthy and N.A. Molloy, Chem. Eng. J., 7 (1974) 1.
4 M. Goldin, H. Yerushalmi, R. Pfeffer and R. Shinnar, J. Fluid Mech., 38 (1969) 689.
5 J.S.W. Rayleigh, Proc. Lond. Math. Soc., 10 (1878) 4.
6 D.B. Bogy, Phys. Fluids, 21 (1978) 190.
7 A.E. Green, Int. J. Engng Sci., 14 (1976) 49.
8 S. Middleman, Chem. Engng Sci., 20 (1965) 1037.
9 S.L. Goren and M. Gottlieb, J. Fluid Mech., 120 (1982) 245.
10 R. Keunings, J. Comp. Physics, 62 (1986) 199.
11 M.M. Denn, in: J.R.A. Pearson and S. Richardson (Eds.), Computational Analysis of Polymer Processing, Applied Science Publishers, London, 1983, p. 179.
12 D.W. Bousfield, G. Marrucci and M.M. Denn, in: B. Mena, A. García-Rejón and C. Rangel-Nafaille (Eds.), Proc. IX Intl. Congress on Rheology, 1984, Vol. 2, p. 239. Distributed by Elsevier, Amsterdam.
13 R. Keunings, in: B. Mena, A. García-Rejón and C. Rangel-Nafaille (Eds.), Proc. IX Intl. Congress on Rheology, 1984, Vol. 1, p. 699. Distributed by Elsevier, Amsterdam.
14 E.F. Goedde and M.C. Yuen, J. Fluid Mech., 40 (1970) 495.
15 H.H. Taub, Phys. Fluids, 19 (1976) 1124.
16 M.C. Yuen, J. Fluid Mech., 33 (1960) 151.
17 D.F. Rutland and G.S. Jameson, Chem. Eng. Sci., 25 (1970) 1689.
18 P. Lafrance, Phys. Fluids, 18 (1975) 428.
19 M. Gordon, J. Yerushalmi and R. Shinnar, Trans. Soc. Rheol., 17 (1973) 303.
20 R. Chin, M.S. Thesis, U.C. Berkeley, 1982.
21 M.M. Denn and G. Marrucci, AICHE J., 17 (1971) 101.
22 M.C. Williams, AICHE J., 21 (1975) 6.
23 D.W. Bousfield and M.M. Denn, Chemical Engineering Communications, to be published (1986).
24 D.V. Boger and M.M. Denn, J. Non-Newtonian Fluid Mechanics, 6 (1980) 163.
25 D.W. Bousfield, Ph.D. Thesis, in preparation.